Chapter 3
Connection Between Microscopic and Macroscopic Models

Jan-Frederik Pietschmann

Abstract This chapter is devoted to the detailed study of the relation between a microscopic cellular automation and a macroscopic partial differential equation model for the movement of pedestrians. We describe the mathematical tools allowing to derive the macroscopic from the microscopic model. Such a connection between discrete, particle based and continuous, density based models can help to improve the understanding of basic properties of human crowds. We exemplify this by applying our results to typical cases. The first one is the formation of lanes in bi-directional flow. The second is the analysis of the fundamental diagram. Our analysis provides (at least qualitatively) a connection between these phenomena and model parameters. We conclude by pointing out a number of possible directions of future research.

3.1 Introduction

A good understanding of the collective behavior of large human crowds (crowd motion) is of importance for several reasons. First of all, a growing fraction of humanity is living in urban regions. These regions especially include facilities such as airports or shopping malls in which a large number of people is concentrated in a relatively small place. Appropriate mathematical models can help to optimize these buildings in order to avoid congestion and allow for faster operation. Even more important, they can be used to create and validate (using numerical simulations) evacuation plans which are of course of highest importance.

Therefore the ultimate goal in terms of mathematical modeling is to develop a model which is able to describe (at least qualitatively) the behavior of human

J.-F. Pietschmann (✉)
Numerical Analysis and Scientific Computing, Department of Mathematics, TU Darmstadt, Dolivostr. 15, 64293 Darmstadt
e-mail: pietschmann@mathematik.tu-darmstadt.de

S. Ali et al. (eds.), *Modeling, Simulation and Visual Analysis of Crowds*, The International Series in Video Computing 11, DOI 10.1007/978-1-4614-8483-7_3,

crowds over a large range of situations. Such a model does not yet exist and in the following we shall outline the difficulties in creating it. A major issue here is obviously the complexity of the humans involved. Their behavior depends on the individual characteristics of each agent such as age, height, sex or even cultural heritage [8]. Furthermore the behavior of each individual may change drastically depending on the situation (e.g. normal walking versus panic). However, even if it is assumed that all people behave exactly the same way, the situation remains complicated. This becomes clearer by comparing a human crowd with a multi particle system from physics (e.g. an electron gas or a plasma). The usual strategy in physics to understand these complex systems is to start from a simple case, i.e. the interaction between only two particles. This process is governed by a simple physical law which then acts as a starting point for the understanding of the complete system using certain mathematical tools. In crowd motion, however, the interaction of a small number of people is already difficult to understand and therefore the principle "from simple to complex" is not applicable. As a result, most existing models are built upon simplified hypotheses and are mostly phenomenological.

3.2 Related Work

In crowd modelling, one can distinguish between two general approaches: microscopic and macroscopic models. In the microscopic framework, people are treated as individual entities (particles). The evolution of the particles in time is determined by physical and social laws which describe the interaction among the particles as well as their interactions with the physical surrounding. Examples for microscopic methods are social force models (see [17] and the references therein), cellular automata, [12, 28], queuing models, [40], or continuum dynamic approaches like [37]. Social force models are also popular in computer vision, see [24, 27, 30, 39]. For an extensive review of different microscopic approaches we refer to [14]. In contrast to microscopic models, macroscopic models treat the whole crowd as an entity without considering the movement of single individuals. The crowd is often represented by a density function depending on ('continuous') space and time. Classical approaches use well known concepts from fluid or gas dynamics, see [18]. More recent models are based on optimal transportation methods [26], mean field games, cf. [22] (see [23] for a general introduction) or non-linear conservation laws [11]. In [31], an approach based on time-evolving measures is presented. We finally note that crowd motion models share many features with traffic models, cf. [2].

We remark that, that due to the difficulties mentioned above, there is in many cases no connection between microscopic and macroscopic models. However, such an approach would be useful: While microscopic models are closest to observations and are a very intuitive approach, many interesting quantities (such as density or velocity) are macroscopic. Also collective self-organization phenomena (e.g. lane formation) appears on a macroscopic scale.

In this work we describe in detail how such a connection can be derived between a cellular automaton model introduced in [21] and a system of partial differential equations similar to the ones in [4, 6]. We will discuss lane formation and the analysis of the fundamental diagram as two possible applications.

3.2.1 Notation

Throughout this chapter we use the following notation:

$\mathbb{R}$	Set of real numbers,
$\mathbb{R}^+$	Set of positive real numbers,
$\mathbb{N}$	Set of positive integers,
∂_t	partial derivative with respect to t,
∇	Vector containing all partial derivatives with respect to the space variable x, i.e. $\nabla = (\partial_{x_1}, \partial_{x_2}, \ldots, \partial_{x_n})^T$ for $x \in \mathbb{R}^n$,
$\nabla\cdot$	divergence operator, i.e. for $V = (V_1, \ldots, V_n)^T \in \mathbb{R}^n$ we have $\nabla \cdot V(x) = \sum_{i=1}^n \partial_{x_i} V_i(x)$, $x \in \mathbb{R}^n$
∇^2	The Laplace operator, i.e. $\nabla^2 u(x) = \sum_{i=1}^n \partial_{x_i x_i} u(x)$.

3.3 The Microscopic Model for Two Species

We start from a cellular automaton model for human crowd motion introduced in [21]. The model is based on an asymmetric simple exclusion process (ASEP) on a two-dimensional grid of size $m_x \cdot n_y$ (the size of one cell is typically about $40 \times 40\,\mathrm{cm}^2$, cf. [33], originating from a maximal density of 6.25 people per m^2, cf. [38]). Given a discrete time step, the model provides for each individual in a given cell the probability to jump into a neighboring cell. This probability is determined by several factors: First of all, individuals are not allowed to jump to an occupied cell (size exclusion, cf. [36]). Furthermore, there exist two driving forces, called "floor fields", cf. [7], a static field S and a dynamic field D on which the jump-probability depends exponentially. The static field S provides individuals with a sense of their environment, increasing towards locations they want to reach, such as doors. The dynamic field D is created by the particles themselves and accounts for herding effects. This is a key feature of the model and one goal of this chapter is to examine its impact on the formation of lanes. Being zero at the initial time, the value of D is increased whenever a particle leaves a cell, modeling the tendency of people to follow others. Note that the concept of floor fields is also used in computer vision, cf. [1]. It is straightforward to extend this model to multiple species, each of them coupled to its own dynamic and static field. In the following, we consider the case of two species (labeled red or r and blue or b). For simplicity, we shall only explain the model for particles of group r with corresponding fields D_r and S_r. The probability of a particle to jump into a neighboring cell i, j is given by

$$(P_r)_{i,j} = (N_r)_{i,j} \exp\left(k_D\,(D_r)_{i,j}\right) \exp\left(k_S (S_r)_{i,j}\right)(1 - r_{i,j} - b_{i,j}). \tag{3.1}$$

The term $(1 - r_{i,j} - b_{i,j})$ accounts for the size exclusion effect rendering the probability zero if a cell is occupied. The positive constants k_D and k_S regulate the relative influence of the two floor fields. Finally, $(N_r)_{i,j}$ is a normalization factor given by

$$(N_r)_{i,j}^{-1} = \sum_{k=\{i-1,i+1\}} \sum_{l=\{j-1,j+1\}} e^{k_D (D_r)_{k,l}} e^{k_S (S_r)_{k,l}}. \tag{3.2}$$

The dynamic field D_r is zero at the beginning of a simulation. In every step, it is updated using the following rules

- It is increased by one whenever a particle left a cell, i.e.

$$(D_r)_{i,j}^{k+1} = \begin{cases} (D_r)_{i,j}^{k} + 1 \text{ if } (r_{i,j}^{k} - r_{i,j}^{k+1}) = 1 \\ (D_r)_{i,j}^{k} \qquad \text{otherwise} \end{cases} \tag{3.3}$$

- If $D_r \geq 1$, it decreases by a given probability $\delta > 0$, i.e. given a random number p

$$(D_r)_{i,j}^{k+1} = \begin{cases} (D_r)_{i,j}^{k} - 1 \text{ if } p < \delta \\ (D_r)_{i,j}^{k} \qquad \text{otherwise} \end{cases} \tag{3.4}$$

- The diffusion is implemented in the following way: With a probability of $\kappa/4$, $\kappa \in \mathbb{R}^+$ a particle jumps to one of its neighboring fields. With probability $(1 - \kappa)$, it stays at its place.

Note that these rules imply that the value of D_r is always a non-negative integer.

3.4 Derivation of the Macroscopic Model

In this section we describe the derivation of a (system of) partial differential equations from the modified ASEP introduced above, cf. [4,36]. The resulting model is macroscopic is the following sense: In the ASEP, pedestrians are represented by particles and at each time step, the position of each particle is known. On the contrary, the PDE model describes the evolution of densities. These densities can be understood as the average number of pedestrians at a certain point in time and space. Therefore, this model is not able to produce trajectories of individual pedestrian. On the other hand, due to the intrinsic averaging, global quantities (which are for example necessary to compute the fundamental diagram) can be extracted easily.

For the sake of clarity, we perform the derivation in one space dimension only. It is analogous in higher dimensions.

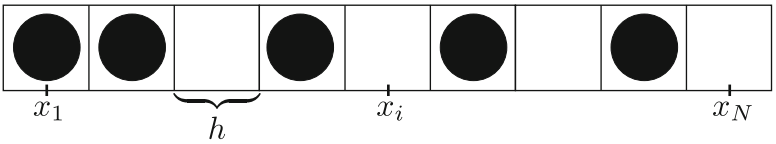

Fig. 3.1 The microscopic setting in one space dimension

3.4.1 Setup

In one space dimension, the model reduces to a row of N cells of width h, as shown in Fig. 3.1. We scale the width of the cells such that the total length of the row is one, i.e. chose h such that $hN = 1$. Furthermore, we denote by x_i the midpoint of cell i, $i = 1, \ldots, N$. In the microscopic model, all quantities are discrete: r_i and b_i denote the number of red and blue particles in cell i, respectively. The values of the floor fields are assumed to be constant in each cell resulting in a finite number of values S_i and D_i. On the other hand, the densities appearing in the macroscopic model are functions of continuous space and time variables ($x \in [0,1]$, $t \in \mathbb{R}^+$). Therefore, we introduce the functions

$$\begin{array}{llll} \tilde{S}_r & : [0,1] & \to \mathbb{R}^+ & \tilde{S}_b \; : [0,1] \quad \to \mathbb{R}^+ \\ \tilde{D}_r & : [0,1] \times \mathbb{R}^+ & \to \mathbb{R}^+ & \tilde{D}_b \; : [0,1] \times \mathbb{R}^+ \to \mathbb{R}^+ \\ \tilde{r} & : [0,1] \times \mathbb{R}^+ & \to [0,1] & \tilde{b} \quad : [0,1] \times \mathbb{R}^+ \to [0,1]. \end{array} \tag{3.5}$$

To connect these functions with their discrete analogues (i.e. $\tilde{S}$ with S_i, $\tilde{D}$ with D_i, etc.), we define them as constant on each cell. For example

$$\tilde{S}_r(x) = \begin{cases} S_1, & \text{if } 0 \le x < h, \\ \ldots, & \\ S_i, & \text{if } hi \le x < h(i+1), \\ \ldots. & \end{cases} \tag{3.6}$$

In other words, the functions are piecewise constant and in each cell attain the value of their discrete analogue. With these definitions, the probability of a particle to jump into the cell with midpoint x_i is given by

$$\tilde{P}_c(x_i, t_k) = N e^{k_{D_c} \tilde{D}_c(x_i,t_k)} e^{k_{S_c} \tilde{S}_c(x_i)} (1 - \tilde{r}_i(x_i,t_k) - \tilde{b}_i(x_i,t_k)), \quad c = r, b, \tag{3.7}$$

with

$$\tilde{N}_c(x_i, t_k) = \frac{1}{\sum_{k=i-1}^{i+1} e^{k_{D_c} \tilde{D}_c(x_i,t_k)} e^{k_{S_c} \tilde{S}_c(x_i)}}, \quad c = r, b.$$

Note that even though these expressions look very similar to (3.1) and (3.2) they are different as they are valid for arbitrary $x \neq x_i$, $i = 1, \ldots, N$ and $t \neq t_k$, $k \in \mathbb{N}_+$.

Closure Assumption A priori, only $n_{i,j}$, i.e. the information whether cell (i,j) is occupied or not is known. However, in (3.7) we replaced $n_{i,j}$ by $\tilde{r}_i(x_i,t_k)+\tilde{b}_i(x_i,t_k)$, i.e. the **probability** of the cell being occupied or not. This is needed to obtain a closed equation and therefore called a "closure assumption". In cases in which the macroscopic limit can be justified rigorously, this closure assumption turns out to be the right one, cf. [13], which motivates our choice.

3.4.2 Master Equation

We will now formulate the dynamics of the macroscopic model by using a so-called master-equation, see for example [3]. This equation describes how the probabilities to find a particle in a certain cell evolve in time. To increase readability, we will neglect the tildes from the previous section and write r, b, S, D instead of $\tilde{r}, \tilde{b}, \tilde{S}, \tilde{D}$. For red and blue particles, the corresponding master equations are given by

$$\begin{aligned} r(x_i,t_{k+1}) &= P_r(x_i,t_k)(r(x_{i-1},t_k)+r(x_{i+1},t_k)) \\ &\quad + r(x_i,t_k)(1-P_r(x_{i-1},t_k)-P_r(x_{i+1},t_k)), \end{aligned} \tag{3.8}$$

$$\begin{aligned} b(x_i,t_{k+1}) &= P_b(x_i,t_k)(b(x_{i-1},t_k)+b(x_{i+1},t_k)) \\ &\quad + b(x_i,t_k)(1-P(x_{i-1},t_k)-P(x_{i+1},t_k)), \end{aligned} \tag{3.9}$$

These equations states the probability of finding a particle at position x_i at time t_{k+1} given the state of the system at time t_k. Since the ASEP allows particles to jump only one cell per time step, we only need to take the cells i, $i-1$ and $i+1$ into account. Roughly speaking, the master equation consists of two terms: The probability of a particle at cell $i\pm 1$ to jump into cell i (first term) and probability for a particle to stay in cell i (i.e. one minus the probability to jump out of the cell, second term). Note that since the probabilities are real numbers in $[0,1]$, the values of r and b do not need to be discrete integers anymore. For corresponding equations for the dynamic fields read as

$$\begin{aligned} D_r(x_i,t_{k+1}) &= D_r(x_i,t_k)+(\Delta t)r(x_i,t_k)(P_r(x_{i-1},t_k)+P_r(x_{i+1},t_k)) \\ &\quad -\delta D_r(x_i,t_k), \end{aligned} \tag{3.10}$$

$$\begin{aligned} D_b(x_i,t_{k+1}) &= D_b(x_i,t_k)+(\Delta t)b(x_i,t_k)(P_b(x_{i-1},t_k)+P_b(x_{i+1},t_k)) \\ &\quad -\delta D_b(x_i,t_k). \end{aligned} \tag{3.11}$$

i.e. value of D increases, whenever a particle leaves an occupied field and decreases with rate $\delta>0$.

We are now ready to perform the limiting procedure which transforms the ASEP into a system of partial differential equations. We will only consider red particles from now on as the strategy is exactly the same for the blue ones. The mathematical strategy to obtain the microscopic model is to perform the limit $\Delta t \to 0$, $h \to 0$. In other words: We let the width of the cells and the length of the discrete time steps tend to zero. Since the total length is fixed by $hN = 1$ this means that the number of cells tend to infinity. If we multiply the master equation for r, (3.8), by $\frac{1}{\Delta t}$ we obtain

$$\begin{aligned}\frac{1}{\Delta t}\left(r(x_i,t_{k+1}) - r(x_i,t_k)\right) = \frac{1}{\Delta t}\big(&P_r(x_i,t_k)(r(x_{i-1},t_k) + r(x_{i+1},t_k)) \\ &+ r(x_i,t_k)(1 - P_r(x_{i-1},t_k) - P_r(x_{i+1},t_k))\big),\end{aligned}$$

we see that in the limit $\Delta t \to 0$, the left hand side will converge to $\partial_t r$. However, the resulting equation is still discrete in space and it is not clear what happens to the right hand side in the limit. We therefore perform a Taylor expansion of the right hand side around x_i. Remember that we are planing to let h tend to zero, therefore it is reasonable to assume it to be small which justifies the Taylor expansion. We first take a closer look at Eq. (3.12). Taylor expansion of the right hand side around the point $x = x_i$ yields

$$\begin{aligned}&r(x_i,t+\Delta t) - r(x_i,t) \\ &= h^2 P(x_i,t)\partial_x r(x_{i+1},t) - h^2 r(x_i,t)\partial_x P(x_{i+1},t) \\ &= h^2 P(x_i,t)\partial_x r(x_i,t) - h^2 r(x_i,t) \\ &\quad \partial_x\left(N e^{k_{S_r} S_r} e^{k_{D_r} D_r}\left[(1 - r(x_i,t))(\partial_x D + \partial_x S) - \partial_x r(x_i,t)\right]\right) \\ &= h^2 \partial_x\left(N e^{k_{S_r} S_r} e^{k_{D_r} D_r} \partial_x r(x_i,t)\right) \\ &\quad - h^2 \partial_x\left(N e^{k_{S_r} S_r} e^{k_{D_r} D_r} r(x_i,t)(1 - r(x_i,t))(\partial_x D + \partial_x S)\right).\end{aligned}$$

The final step before we actually pass to the limit is to chose the relation between Δt and h, the so-called scaling, [13]. If we divide again by Δt, we see that the quantity $\frac{h^2}{\Delta t}$ appears on the right hand side. Thus we chose $\frac{h^2}{\Delta t} =: P = \text{const} > 0$. The constant P acts as a diffusion coefficient. Then, the left hand side will converge to the time derivative $\partial_t r$, while the right hand side does not depend on h or Δt anymore (up to higher order terms which vanish as $h \to 0$). Thus passing to the limit $h, \Delta t \to 0$ we obtain

$$\partial_t r + \frac{P}{3}\partial_x\left(r(1-r)\left(k_{S_r}\partial_x S_r + k_D \partial_x D_r\right)\right) = \frac{P}{3}\partial_{xx} r. \tag{3.12}$$

We made use of the fact that

$$F_i(h^2) := e^{k_{D_r} D_r(x_i)} e^{k_{S_r} S_r(x_i,t)} N_i = \frac{e^{k_{D_r} D_r(x_i,t)} e^{k_{S_r} S_r(x_i)}}{3 e^{k_{D_r} D_r(x_i,t)} e^{k_{S_r} S_r(x_i)} + \mathcal{O}(h^2)} \xrightarrow{h\to 0} \frac{1}{3}. \tag{3.13}$$

For (3.10), we apply the same procedure yielding

$$\begin{aligned}
&\frac{D_r(x_i,t+\Delta t) - D_r(x_i,t)}{\Delta t} \\
&\quad = r_i(t)(P(x_{i+1},t) + P(x_{i-1},t)) - \delta D_r(x_i,t_k) \\
&\quad = r(x_i,t)(F_{i+1}(h^2)(1 - r(x_{i+1},t) + F_{i-1}(h^2)(1 - r(x_{i-1},t)) - \delta D_r(x_i,t_k) \\
&\quad = r(x_i,t)\left(F_{i+1}(h^2)(1 - r(x_i,t) + F_{i-1}(h^2)(1 - r(x_i,t)\right) - \delta D_r(x_i,t_k) \\
&\qquad + r(x_i,t)\left(h\left(F_{i+1}(h^2)\frac{\partial r(x_i,t)}{\partial x} - F_{i-1}(h^2)\frac{\partial r(x_i,t)}{\partial x}\right)\right) - \delta D_r(x_i,t_k) \\
&\qquad + \mathcal{O}(h^2)
\end{aligned}$$

In the limit $\Delta t,\ h^2 \to 0$, the last term on the right hand side vanishes and we obtain

$$\partial_t D_r = -\delta D_r + \frac{2}{3} r(1-\rho).$$

As it is well known, cf. [9, 10], that the diffusion algorithm described in Sect. 3.3 yields, in the continuum limit a term $\kappa \partial_{xx} D_r$, we arrive at

$$\partial_t D_r = \kappa \partial_{xx} D_r - \delta D_r + \frac{2}{3} r(1-\rho). \tag{3.14}$$

3.4.3 The Macroscopic PDE Limit

As the limiting procedure can be performed in arbitrary spatial dimensions, we finally obtain the following non-linear Nernst-Planck type equations for the densities r and b

$$\partial_t r = \nabla \cdot P((1-\rho)\nabla r + r\nabla\rho + r(1-\rho)\nabla(k_{S_r} S_r + k_{D_r} D_r)), \tag{3.15}$$

$$\partial_t b = \nabla \cdot P((1-\rho)\nabla b + b\nabla\rho + b(1-\rho)\nabla(k_{S_r} S_b + k_{D_r} D_b)), \tag{3.16}$$

coupled to

$$\partial_t D_r = \kappa \nabla^2 D_r - \delta_1 D_r + r(1-\rho), \tag{3.17}$$

$$\partial_t D_b = \kappa \nabla^2 D_b - \delta_1 D_b + b(1-\rho), \tag{3.18}$$

with $x \in \Omega \subset \mathbb{R}^n, t > 0$. Appropriate initial and boundary conditions depend on the application and will be discussed below. We remark that neglecting the dynamic fields, this model has been analyzed extensively in [4,5].

3.5 Application I: Linear Stability Analysis and the Formation of Lanes

Video recordings of real crowds show that they exhibit a wide range of what is called *collective phenomena*. One common example among them is *lane formation*, see for example [15] and [17]. Pedestrians with the same desired walking direction prefer to walk in lanes. Typically, the number of lanes depends on the width of the street and on the density of pedestrians. One possible explanation for lane formation is as follows: Pedestrians walking against the stream have a high relative velocity. As a consequence, these pedestrians change their walking direction sideways to avoid collisions, which finally leads to separation [16]. The formation of lanes for two species (but without static field) has already been briefly demonstrated numerically in [32]. In this section, we provide simulation results of the microscopic model demonstrating the occurrence of lanes. This motivates the use linear stability analysis of our macroscopic model (3.15)–(3.18) to obtain insight into the role of the dynamic fields in this process.

3.5.1 Monte Carlo Simulations

We performed simulations of the above model on a 20×100 cell grid. We used a Mersenne twister, cf. [25], to create the pseudo-random numbers needed. The main issue here is to deal with so-called "conflicts", i.e. the case when two particles want to jump into the same cell. In our implementation, we followed the strategy described in [20]. The basic idea is the following: A new parameter $\lambda \in [0,1]$ in introduced. If two or more particles want to jump to the same cell, this new parameter determines their behavior: With probability λ, none of the particles jumps and the cell remains empty. With probability $(1-\lambda)$, one particle is chosen randomly and jumps into the target cell. In our set-up, red particles enter the domain from the left and blue particles from the right. Both species are supplemented with a static field transporting them through the channel. For this simulation, we chose the following parameters: $\delta = 0.05, k_D = 1.0, k_S = 7, \kappa = 0.5$. The diffusion coefficients of r and b are chosen as 0.0005 in x- and 0.1 in y-direction. The boundary conditions are implemented as follows: In each step, for each cell on the left boundary, a random number is generated. If this number is below a given value bc_l, a virtual particle is created. This particle evolves due to the usual probabilities given by the model and can either jump into the domain or vanishes. On

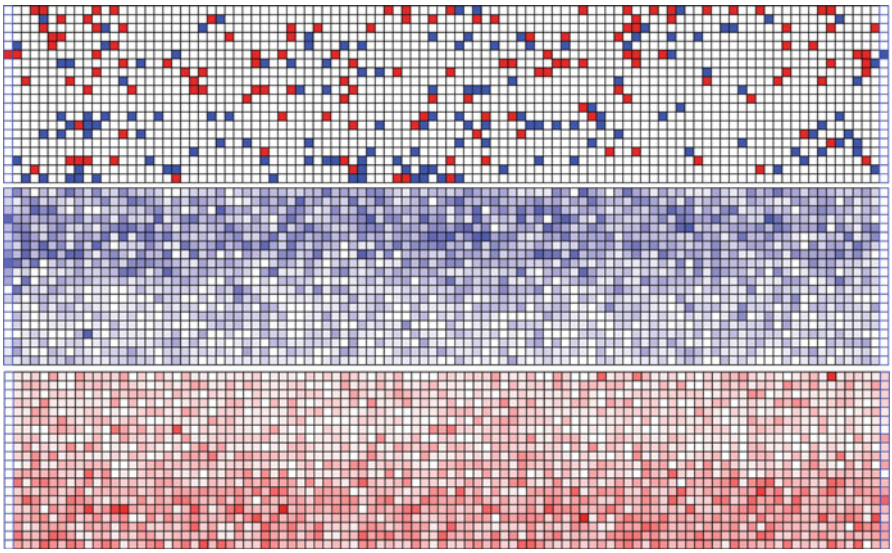

Fig. 3.2 (Color online) Results of the Monte Carlo simulations: Snapshot of a single simulation after 1,000 steps (*top*); density of *red* particles after 2,000 steps, averages over 35 runs (*bottom*); density of *blue* particles after 2,000 steps, averages over 35 runs (*middle*)

the right side, the boundary conditions are implemented in the same way with a corresponding boundary value bc_r. In our experiment, we added small perturbations in y-direction, i.e.

$$bc_l = \tilde{bc}_l + 0.04 \sin\left(\frac{2k\pi}{n_x} i\right), i = 1, \ldots, n_x, \tag{3.19}$$

$$bc_r = \tilde{bc}_r + 0.04 \sin\left(\frac{2k\pi}{n_x} i + \pi\right), i = 1, \ldots, n_x. \tag{3.20}$$

Here, we chose $\tilde{bc}_l = \tilde{bc}_r = 0.06$. In Fig. 3.2 (top), we show a snapshot of one simulation demonstrating the formation of two lanes. Figure 3.2 (bottom), we show the average density of red particles at step 2,000 averages over 35 simulations, in Fig. 3.2 (middle), we same is shown for the blue species.

3.5.2 Linear Stability Analysis

The idea is as follows: We consider an equilibrium state of the system in which both red and blue particles are uniformly distributed within the whole domain. Then, we add a small, asymmetric perturbation and observe the system's reaction as time evolves. The question is under which conditions the perturbations do not smooth

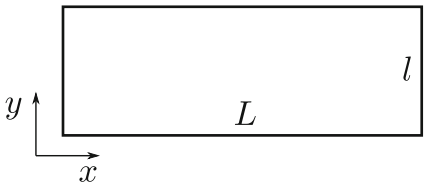

Fig. 3.3 Geometry of the domain on which the linear stability analysis is performed

out, but grow in time. The procedure is summarized in Fig. 3.4. We remark we do not assume that individuals have a tendency to prefer a special walking site.

To be able to obtain an explicit condition, we make the following assumptions:

- The static floor fields are acting only in x-direction, we assume the special case

$$\nabla S_r = (1,0), \quad \nabla S_b = (-1,0), \tag{3.21}$$

  meaning that the red and blue individuals have opposite preferred walking directions.
- The diffusion of particles in x-directions vanishes, which is reasonable in case of pedestrians walking along a corridor, as it is unlikely for them to go randomly forward or backward.
- The diffusion of the dynamic floor fields D_c, $c = r,b$ vanishes in y-direction, corresponding to small movements orthogonal to the walking direction.
- The evolution of the dynamic floor fields is slow compared to that of the densities r and b. Therefore, we only consider the stationary version of (3.17) and (3.18).
- The coupling constants to static and dynamic field are equal for both species, i.e.

$$k_{S_r} = k_{S_b} = k_S, \quad k_{D_r} = k_{D_b} = k_D.$$

- All calculations are performed on the two-dimensional domain $\Omega = [0,L] \times [0,l] \subset \mathbb{R}^2$ depicted in Fig. 3.3.

Under these assumptions, Eqs. (3.15)–(3.18) reduce to

$$\begin{aligned}\partial_t r =& P\partial_y\left((1-b)\partial_y r + r\partial_y b\right) + Pk_S\partial_x(r(1-\rho)) + Pk_D\nabla(r(1-\rho)\nabla D_r) \qquad (3.22)\\ =& \nabla\cdot(-J_r)\\ \partial_t b =& P\partial_y\left((1-r)\partial_y b + b\partial_y r\right) - Pk_S\partial_x(b(1-\rho)) + Pk_D\nabla(b(1-\rho)\nabla D_b) \qquad (3.23)\\ =& \nabla\cdot(-J_b),\\ 0 =& \kappa\partial_{xx}D_r - \delta_1 D_r + r(1-\rho), \qquad (3.24)\\ 0 =& \kappa\partial_{xx}D_b - \delta_1 D_b + b(1-\rho) \qquad (3.25)\end{aligned}$$

Hence, the total flux of red and blue particles, respectively, is given by

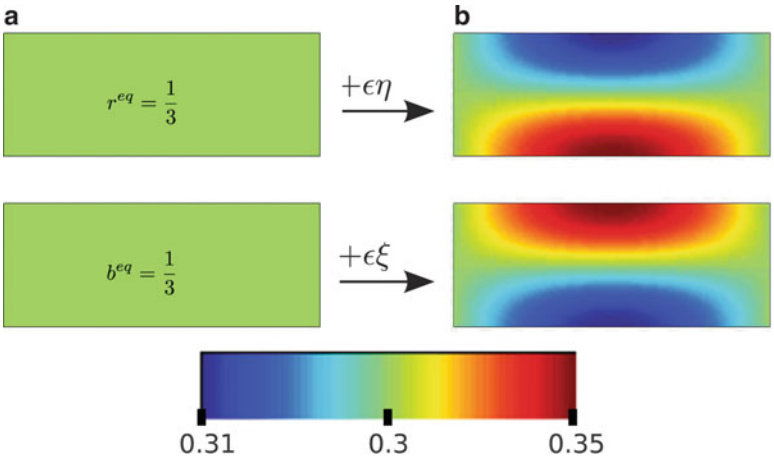

Fig. 3.4 (**a**) Constant densities r^{eq}, b^{eq}, (**b**) small perturbations $\varepsilon\xi$ and $\varepsilon\eta$ added

$$J_r = -P\begin{pmatrix} k_S r(1-b) + k_D(r(1-\rho)\partial_x D_r \\ (1-b)\partial_y r - r\partial_y \rho + k_D(r(1-\rho)\partial_y D_r \end{pmatrix},$$

and

$$J_b = -P\begin{pmatrix} k_S b(1-r) + k_D(b(1-\rho)\partial_x D_b \\ (1-r)\partial_y b - b\partial_y \rho + k_D(b(1-\rho)\partial_y D_b \end{pmatrix}.$$

We supplement this system with the following boundary conditions: We assume constant influxes of r and b at the left or right end of the corridor, respectively. Furthermore, we say that the particles are leaving the domain at with a constant velocity v_0 and with a rate proportional to their density. This leads to

$$J_r \cdot \begin{pmatrix} -1 \\ 0 \end{pmatrix} = J_r^{in} = \text{const and } J_b \cdot \begin{pmatrix} -1 \\ 0 \end{pmatrix} = bv_0.$$

At $x = L$, we obtain

$$J_r \cdot \begin{pmatrix} 1 \\ 0 \end{pmatrix} = rv_0 \text{ and } J_b \cdot \begin{pmatrix} 1 \\ 0 \end{pmatrix} = J_b^{in} = \text{const.}$$

We assume no-flux boundary conditions in y-direction:

$$J_r \cdot \begin{pmatrix} 0 \\ 1 \end{pmatrix} = J_b \cdot \begin{pmatrix} 0 \\ 1 \end{pmatrix} = 0 \qquad \text{for } y = 0, l,$$

meaning that particles can only enter or leave the corridor though the left or right entrance. Now we are able to perform the linear stability analysis explained above: We call the constant equilibrium states r^{eq} and b^{eq} as well as D_r^{eq} and D_b^{eq}. Then we add the following perturbations:

$$\begin{aligned} r^{eq} &\to r^{eq} + \varepsilon\xi, & b^{eq} &\to b^{eq} + \varepsilon\eta, \\ D_r^{eq} &\to D_r^{eq} + \varepsilon\Psi_r, & D_b^{eq} &\to D_b^{eq} + \varepsilon\Psi_b, \end{aligned}$$

where $\xi(x,t)$, $\eta(x,t)$, $\Psi_r(x,t)$ and $\Psi_b(x,t)$ denote the time and space dependent perturbations and $\varepsilon \ll 1$. If we insert this ansatz into the system of equations (3.22)–(3.25) (with given external potentials) and neglect all terms of order ε^2 and higher (first order approximation), we obtain the following linear system describing the evolution of the perturbations:

$$\begin{aligned} \partial_t\xi =& P((1-b^{eq})\partial_{yy}\xi - r^{eq}\partial_{yy}\eta) + Pk_S\partial_x((1-\rho^{eq})\xi - r^{eq}(\xi-\eta)) \\ &+ Pk_D r^{eq}(1-\rho^{eq})(\partial_{xx}+\partial_{yy})\Psi_r, \\ \partial_t\eta =& P((1-r^{eq})\partial_{yy}\eta - b^{eq}\partial_{yy}\xi) - Pk_S\partial_x((1-\rho^{eq})\eta - b^{eq}(-\xi+\eta)) \\ &+ Pk_D b^{eq}(1-\rho^{eq})(\partial_{xx}+\partial_{yy})\Psi_b, \\ 0 =& \kappa\partial_{xx}\Psi_r - \delta\Psi_r + (1-\rho^{eq}-r^{eq})\xi + r^{eq}\eta, \\ 0 =& \kappa\partial_{xx}\Psi_b - \delta\Psi_b + (1-\rho^{eq}-b^{eq})\eta + b^{eq}\xi. \end{aligned}$$

The first two equations of this system can be written in the form

$$\partial_t \begin{pmatrix} \xi \\ \eta \end{pmatrix} = A \begin{pmatrix} \xi \\ \eta \end{pmatrix},$$

with a 2×2 matrix A that depends on P, r^{eq}, b^{eq}, k_{S_r}, k_{S_b}, k_{D_r}, k_{D_b}, κ and δ. From this representation it is clear that the evolution of ξ and η is determined by the largest eigenvalue of A: If it is negative, ξ and η will converge to zero as $t \to \infty$ meaning that the system will return to its constant stationary state. If the eigenvalue is positive, ξ and η will stay positive which corresponds to the formation of lanes. In order to calculate an explicit condition for the sign of the eigenvalues, we consider cosinusoidal shaped perturbation in the y direction (as depicted in Fig. 3.4), hence the number of (possible) lanes is given by the mode of the cosine. We are able to predict for several densities and geometries of the domain how many lanes are formed.

The detailed derivation of this condition and the condition itself is stated in the appendix. In the following, we will use it to analyze to interesting special cases.

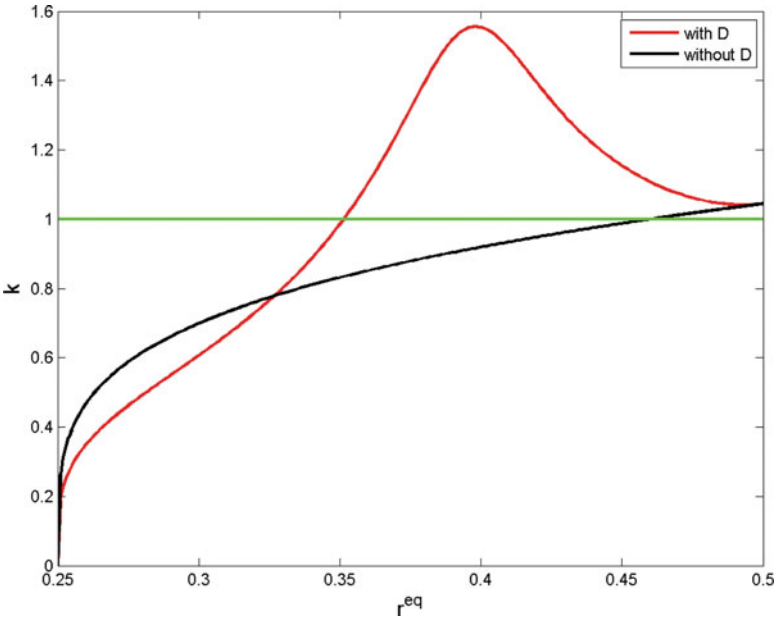

Fig. 3.5 Number of lanes versus density

3.5.3 Number of Lanes for Varying Density

We are able to predict instabilities, thus forming of lanes and the number of lanes, depending on the equilibrium density r^{eq}. In Fig. 3.5, the number of lanes k is plotted versus the density. In this setup, we choose as length l in y-direction to be 7 m. The length L in Fig. 3.5 is 100 m. The decay parameter δ is given by 0.05, and $k_D = 1$. We set $k_S = 7$. Without the dynamic fields D_c, $c = r, b$, (i.e. $k_D = 0$) the first lane in each direction arises at densities of approximately 0.45 in each direction. If we include the dynamic fields, the first lanes are formed at densities of approximately 0.35. Hence, the inclusion of the dynamic fields leads increases the tendencies to follow others.

3.5.4 Number of Lanes for Varying Length

Figure 3.6 shows the number of lanes plotted versus channel length L. We chose the same parameters as before, the density is set to $r^{eq} = 0.33$. It is obvious that the herding behavior does not lead to an increase in the number of lanes. As expected, the tendency to follow others is more pronounced, resulting in less lanes.

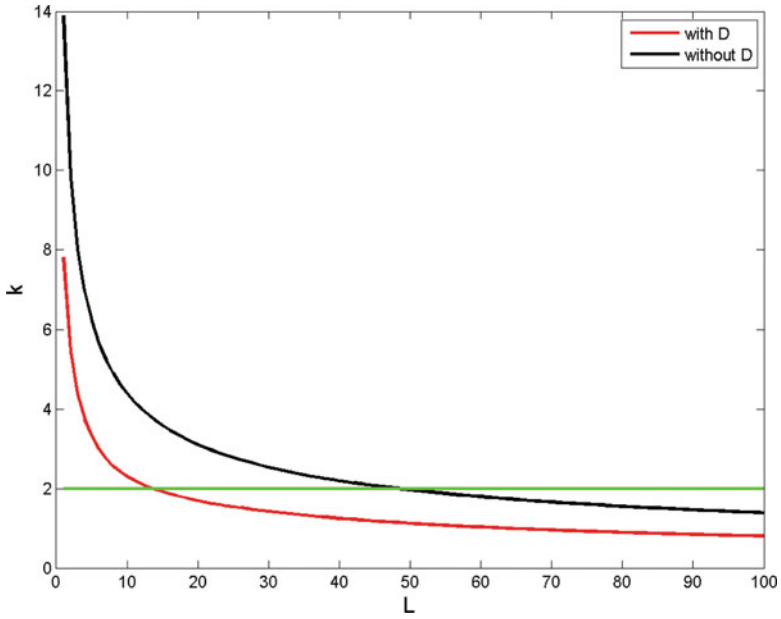

Fig. 3.6 Number of lanes versus length L

3.6 Application II: The Fundamental Diagram

The relation between density ρ and velocity v or total flux (or flow) j, also known as *fundamental diagram*, is a key property of pedestrian movement, [34, 35]. In particular, it can be used to estimate the capacity of facilities such as corridors or streets. There is a lot of experimental data available for different situations, starting from the classical review of Weidmann [38] up to many more recent studies [8, 19, 35]. Thus, the fundamental diagram can also be used as a test to validate crowd motion models. One advantage of our macroscopic model is that the density-velocity relationship in encoded in the structure of the partial differential equation. If we consider the model for one species, e.g. red particles, only and neglect the dynamic field Eqs. (3.15)–(3.18) reduce to

$$\partial_t r = \nabla^2 r - \operatorname{div}(r(1-r)(k_{S_r}\nabla S_r)). \tag{3.26}$$

This corresponds to a uni-directional flow of one species. In this model, the total flux j is given by

$$j := r(1-r)(k_S \nabla S) - \nabla r.$$

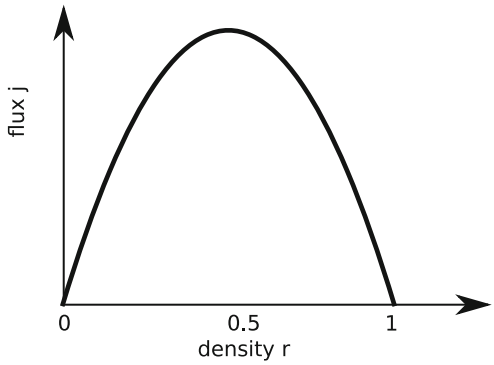

Fig. 3.7 Fundamental diagram for uni-directional flow as predicted by the macroscopic model without dynamic field

Using the relation $r\nabla \ln(r) = \nabla r$, the flux can be rewritten in the form rv, i.e.

$$j = rv = r((1-r)(k_S \nabla S) - \nabla ln(r)).$$

If we assume a constant density r and a constant preferred walking direction ∇S, we recover a linear fundamental diagram $v \sim (1-r)$ and the density-flow relationship is given by $r(1-r)$ as shown in Fig. 3.7. Even though this is far away from detailed experimental results, the key properties are still present: The flow increases with the density until it reaches a maximum. When the density increases further, i.e. the situation becomes more crowded, the individuals are not able to move at their preferred walking speed anymore and the flux decreases until the critical density, at which no movement is possible anymore, is reached. This is of particular interest since situations involving high densities are hard to realize experimentally.

Recent experimental results for bi-directional flow (i.e. two species of people walking in opposite directions), have shown to exhibit a significantly different fundamental diagram compared to uni-directional flow, cf. [41, Fig. 6]. In particular, the maximum is lower but shifted to higher densities. In fact, there seems to be a flat region. One possible explanation is that individuals that are walking towards each other have a stronger dependency to avoid the other. This can easily be incorporated into the microscopic ASEP model by allowing red and blue particles to "switch" their places, as sketched in Fig. 3.8. Such a mechanism is also known from models for intracellular transport, cf. [29]. Thus a rewarding direction of future research is to derive and analyze the corresponding macroscopic formulation for this modified model and compare the resulting fundamental diagram with the experimental results. Another extension is to include the dynamical floor fields and produce fundamental diagrams using numerical simulations.

3.7 Conclusion and Future Work

We established a link between an extended floor field model and a system of non-linear partial differential equations. Using this connection, we were able to give conditions on the formation of lanes depending on the density of particles

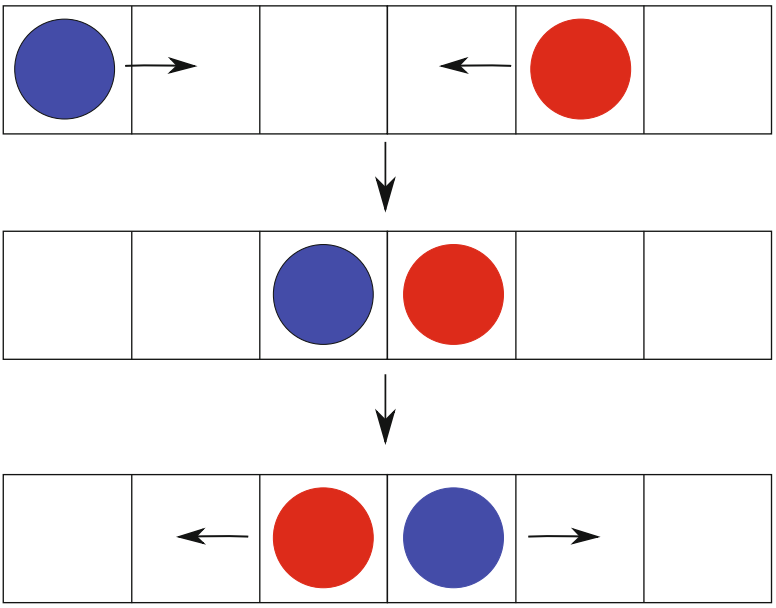

Fig. 3.8 Two particles switching there places in the cellular automata model

as well as the geometry on the domain. The effect of the floor field presenting herding behavior is that lanes are formed at lower densities. A logical next step would be to systematically verify these conditions using the Monte Carlo simulations described above. Also, it would be worthwhile to perform detailed simulations on the macroscopic model (using, e.g. a finite difference scheme) and to compare these results with the microscopic simulations. This would lead to a unified understanding of lane formation in these kind of models. Furthermore, we used the macroscopic description to extract fundamental properties of pedestrian movement, namely the fundamental diagram. We explained how the density-flow relationship can easily be obtained from the macroscopic and briefly mentioned possible extensions to cover recent experimental results regarding bi-directional flow.

Acknowledgements The author acknowledges helpful discussions with M. Burger and B. Schlake (both WWU Münster) as well as A. Seyfried (Jülich/Wuppertal).

Appendix

The linear stability approach described in Sect. 3.5 yields the following linear system for the perturbations

$$\begin{aligned}
\partial_t \xi =& P((1-b^{eq})\partial_{yy}\xi - r^{eq}\partial_{yy}\eta) + Pk_S\partial_x((1-\rho^{eq})\xi - r^{eq}(\xi-\eta)) \\
&+ Pk_D r^{eq}(1-\rho^{eq})(\partial_{xx}+\partial_{yy})\Psi_r, \qquad (3.27)\\
\partial_t \eta =& P((1-r^{eq})\partial_{yy}\eta - b^{eq}\partial_{yy}\xi) - Pk_S\partial_x((1-\rho^{eq})\eta - b^{eq}(-\xi+\eta)) \\
&+ Pk_D b^{eq}(1-\rho^{eq})(\partial_{xx}+\partial_{yy})\Psi_b, \qquad (3.28)\\
0 =& \kappa\partial_{xx}\Psi_r - \delta\Psi_r + (1-\rho^{eq}-r^{eq})\xi + r^{eq}\eta, \qquad (3.29)\\
0 =& \kappa\partial_{xx}\Psi_b - \delta\Psi_b + (1-\rho^{eq}-b^{eq})\eta + b^{eq}\xi. \qquad (3.30)
\end{aligned}$$

We denote length of the domain in y-direction by l, the length in x-direction is denoted by L, see Fig. 3.3. The perturbations are assumed as

$$\xi = U(x)\cos\left(\frac{k\pi}{l}y\right)\exp(\lambda t), \qquad (3.31)$$

$$\eta = V(x)\cos\left(\frac{k\pi}{l}y\right)\exp(\lambda t), \qquad (3.32)$$

$$\Psi_r = Y_r(x)\cos\left(\frac{k\pi}{l}y\right)\exp(\lambda t), \qquad (3.33)$$

$$\Psi_b = Y_b(x)\cos\left(\frac{k\pi}{l}y\right)\exp(\lambda t). \qquad (3.34)$$

where $U(x)$, $V(x)$, $Y_r(x)$ and $Y_b(x)$ denote perturbations in the x-direction, and k denotes the mode of the perturbation in y-direction. From now on, we assume $r^{eq} = b^{eq}$. Inserting this ansatz into Eqs. (3.27) and (3.28) we obtain

$$\begin{aligned}
\lambda/PU =& -(1-r^{eq})\gamma U + r^{eq}\gamma V + k_S(1-3r^{eq})U' + k_S r^{eq}V' \\
&- k_D r^{eq}(1-2r^{eq})(\gamma+\Gamma)Y_r \qquad (3.35)\\
\lambda/PV =& -(1-r^{eq})\gamma V + r^{eq}\gamma U - k_S(1-3r^{eq})V' - k_S r^{eq}U' \\
&- k_D r^{eq}(1-2r^{eq})(\gamma+\Gamma)Y_b, \qquad (3.36)
\end{aligned}$$

where we used $\gamma = \frac{k^2\pi^2}{l^2}$, $'$ denotes the derivative with respect to x, $\Gamma = \frac{\pi^2}{L^2}$ and we assume perturbations Y_i of a sinusoidal or cosinusoidal type $Y_i'' = -\Gamma Y_i$. The equations for U and V finally read, using (3.29) and (3.30):

$$\begin{aligned}
&[\lambda/P + (1-r^{eq})\gamma]U - r^{eq}\gamma V + k_D r^{eq}(1-2r^{eq})\frac{\gamma+\Gamma}{\kappa\Gamma+\delta}[(1-3r^{eq})U + r^{eq}V] \\
&= \quad k_S(1-3r^{eq})U' + \mu r^{eq}V', \qquad (3.37)
\end{aligned}$$

$$[\lambda/P + (1-r^{eq})\gamma]V - r^{eq}\gamma U + k_D r^{eq}(1-2r^{eq})\frac{\gamma+\Gamma}{\kappa\Gamma+\delta}[(1-3r^{eq})V + r^{eq}U]$$
$$= \quad -k_S(1-3r^{eq})V' - \mu r^{eq}U'. \tag{3.38}$$

We denote $\Theta = \frac{\gamma+\Gamma}{\kappa\Gamma+\delta}$. The summation of (3.37) and (3.38) is given by

$$[\lambda/P + (1-2r^{eq})\gamma + k_D r^{eq}(1-2r^{eq})^2\Theta](U+V) \quad = k_S(1-4r^{eq})(U'-V'). \tag{3.39}$$

The derivatives of (3.37) and (3.38) are given by

$$[\lambda/P + (1-r^{eq})\gamma]U' - r^{eq}\gamma V' + k_D r^{eq}(1-2r^{eq})\Theta\left[(1-3r^{eq})U' + r^{eq}V'\right]$$
$$= k_S(1-3r^{eq})U'' + \mu r^{eq}V'', \tag{3.40}$$
$$[\lambda/P + (1-r^{eq})\gamma]V' - r^{eq}\gamma U' + k_D r^{eq}(1-2r^{eq})\Theta\left[(1-3r^{eq})V' + r^{eq}U'\right]$$
$$= -k_S(1-3r^{eq})V'' - \mu r^{eq}U''. \tag{3.41}$$

Subtracting these equation yields

$$[\lambda/P + \gamma + k_D r^{eq}(1-2r^{eq})(1-4r^{eq})\Theta](U'-V')$$
$$= k_S(1-2r^{eq})(U''+V''). \tag{3.42}$$

Combining (3.39) and (3.42) leads to

$$[\lambda/P + (1-2r^{eq})\gamma + k_D r^{eq}(1-2r^{eq})^2\Theta](U+V) = \tag{3.43}$$
$$k_S^2\frac{(1-4r^{eq})(1-2r^{eq})}{\lambda/P + \gamma + k_D r^{eq}(1-2r^{eq})(1-4r^{eq})\Theta}(U''+V'').$$

In the following, we assume perturbations U and V in x-direction of a sinusoidal type, due to the homogeneous boundary conditions. This leads to

$$U'' = -\frac{m^2\pi^2}{L^2}U, \qquad V'' = -\frac{m^2\pi^2}{L^2}V,$$

where L denotes the length of the domain in x direction. In the following, we take $m = 1$, as we are only interested in lanes forming along the x-direction. We finally arrive at

$$0 = [\lambda^2/P^2 + 2\lambda/P[\gamma(1-r^{eq}) + k_D r^{eq}(1-2r^{eq})(1-3r^{eq})\Theta]$$
$$+ \gamma^2(1-2r^{eq}) + 2\gamma k_D r^{eq}(1-2r^{eq})^3\Theta$$
$$+ k_D^2(r^{eq})^2(1-2r^{eq})^3(1-4r^{eq})\Theta^2$$

$$+k_S^2\Gamma(1-4r^{eq})(1-2r^{eq})](U+V). \tag{3.44}$$

Accordingly, the equation for λ is given by

$$\begin{aligned}\lambda_{1/2} =& -P[(1-r^{eq})\gamma+k_D r^{eq}(1-2r^{eq})(1-3r^{eq})\Theta] \\ &\pm P\sqrt{(r^{eq})^2[\gamma-k_D r^{eq}(1-2r^{eq})\Theta]^2-k_S^2\Gamma(1-4r^{eq})(1-2r^{eq})}.\end{aligned} \tag{3.45}$$

The parameter λ is supposed to be real-valued for all k, particularly for $k=1$. From that we conclude

$$(r^{eq})^2[\gamma-k_D r^{eq}(1-2r^{eq})\Theta]^2 \geq k_S^2\Gamma(1-4r^{eq})(1-2r^{eq}). \tag{3.46}$$

As $r^{eq} \leq 1/2$, (3.46) is always fulfilled in case that $r^{eq} \geq 1/4$. This means that instabilities arise only in case $r^{eq} \geq 1/4$. To obtain instabilities increasing in time, $\lambda > 0$ has to be satisfied. This means

$$\begin{aligned}&[(1-r^{eq})\gamma+k_D r^{eq}(1-2r^{eq})(1-3r^{eq})\Theta]^2 \\ &\quad< (r^{eq})^2\gamma^2-2\gamma k_D(r^{eq})^3(1-2r^{eq})\Theta \\ &\quad+k_D^2(r^{eq})^4(1-2r^{eq})^2\Theta^2-k_S^2\Gamma(1-4r^{eq})(1-2r^{eq})\end{aligned} \tag{3.47}$$

Assuming $(1-2r^{eq})>0$, which means that the overall density is below maximum, we obtain

$$\begin{aligned}&\gamma^2+2\gamma k_D r^{eq}(1-2r^{eq})^2\Theta \\ &\quad+k_D^2(r^{eq})^2(1-2r^{eq})^2(1-4r^{eq})\Theta^2+k_S^2\Gamma(1-4r^{eq})<0.\end{aligned} \tag{3.48}$$

The mode of the cosinusoidal perturbation in y-direction is given by k, hence it gives the number of lanes of particles moving in opposite direction which are amplified during time. If $k=1$, we obtain one lane in each direction. Accordingly, we obtain as inequality for $\gamma = \frac{k^2\pi^2}{l^2}$

$$\begin{aligned}&\gamma^2\left[1+2k_D r^{eq}(1-2r^{eq})^2\frac{1}{\kappa\Gamma+\delta}\right. \\ &\quad\left.+k_D^2 r^{eq2}(1-2r^{eq})^2(1-4r^{eq})\frac{1}{(\kappa\Gamma+\delta)^2}\right] \\ &\quad+\gamma\left[2k_D r^{eq}(1-2r^{eq})^2\frac{\Gamma}{\kappa\Gamma+\delta}\right. \\ &\quad\left.+2k_D^2 r^{eq2}(1-2r^{eq})^2(1-4r^{eq})\frac{\Gamma}{(\kappa\Gamma+\delta)^2}\right]\end{aligned}$$

$$+k_D^2 r^{eq\,2}(1-2r^{eq})^2(1-4r^{eq})\frac{\Gamma^2}{(\kappa\Gamma+\delta)^2}+k_S^2\Gamma(1-4r^{eq})$$
$$<0. \tag{3.49}$$

The evaluation of (3.49) leads to a condition on k which determines under which conditions instabilities, which lead to lane formation, appear.

References

1. Ali, S., Shah, M.: Floor fields for tracking in high density crowd scenes. In: ECCV (2), pp. 1–14 (2008)
2. Aw, A., Rascle, M.: Resurrection of "second order" models of traffic flow. SIAM J. Appl. Math. **60**(3), 916–938 (electronic) (2000)
3. Bedeaux, D., Lakatos-Lindenberg, K., Shuler, K.E.: On the relation between master equations and random walks and their solutions. J. Math. Phys. **12**(10), 2116–2123 (1971)
4. Burger, M., Di Francesco, M., Pietschmann, J.-F., Schlake, B.: Nonlinear cross-diffusion with size exclusion. SIAM J. Math. Anal. **42**(6), 2842–2871 (2010)
5. Burger, M., Schlake, B., Wolfram, M.-T. Nonlinear Poisson-Nernst Planck equations for ion flux through confined geometries (2010, preprint)
6. Burger, M., Markowich, P., Pietschmann, J.-F.: Continuous limit of a crowd motion and herding model: analysis and numerical simulations. Kinet. Relat. Models **4**, 1025–1047 (2011)
7. Burstedde, C., Klauck, K., Schadschneider, A., Zittartz, J.: Simulation of pedestrian dynamics using a two-dimensional cellular automaton. Phys. A Stat. Mech. Appl. **295**(3–4), 507–525 (2001)
8. Chattaraj, U., Seyfried, A., Chakroborty, P.: Comparison of pedestrian fundamental diagram across cultures. Adv. Complex Syst. **12**(03), 393–405 (2009)
9. Chopard, B., Droz, M.: Cellular automata model for the diffusion equation. J. Stat. Phys. **64**, 859–892 (1991)
10. Chopard, B., Droz, M.: Cellular Automata Modeling of Physical Systems. Cambridge University Press, Cambridge/New York (2005)
11. Colombo, R.M., Rosini, M.D.: Pedestrian flows and non-classical shocks. Math. Methods Appl. Sci. **28**(13), 1553–1567 (2005)
12. Fukui, M., Ishibashi, Y.: Self-organized phase transitions in CA-models for pedestrians. J. Phys. Soc. Jpn. **8**, 2861–2863 (1999)
13. Giacomin, G., Lebowitz, J.L.: Phase segregation dynamics in particle systems with long range interactions. I. Macroscopic limits. J. Stat. Phys. **87**(1–2), 37–61 (1997)
14. Helbing, D.: Traffic and related self-driven many-particle systems. Rev. Mod. Phys. **73**(4), 1067–1141 (2001)
15. Helbing, D., Molnár, P.: Social force model for pedestrian dynamics. Phys. Rev. E **51**(5), 4282–4286 (1995)
16. Helbing, D., Farkas, I., Vicsek, T.: Freezing by heating in a driven mesoscopic system. Phys. Rev. Lett. **84**, 1240–1243 (2000)
17. Helbing, D., Farkas, I.J., Molnar, P., Vicsek, T.: Simulation of pedestrian crowds in normal and evacuation situations. In: Schreckenberg, M., Sharma, S.D. (eds.) Pedestrian and Evacuation Dynamics, pp. 21–58. Springer, Berlin (2002)

18. Henderson, L.F.: The statistics of crowd fluids. Nature **229**, 381–383 (1971)
19. Hoskin, K.J., Spearpoint, M.: Crowd characteristics and egress at stadia. In: Shields, T.J. (ed.) Human Behaviour in Fire. Intersience, London (2004)
20. Kirchner, A.: Modellierung und statistische Physik biologischer und sozialer Systeme. PhD thesis (in german) (2002)
21. Kirchner, A., Schadschneider, A.: Simulation of evacuation processes using a bionics-inspired cellular automaton model for pedestrian dynamics. Phys. A Stat. Mech. Appl. **312**(1–2), 260–276 (2002)
22. Lachapelle, A., Wolfram, M.-T.: On a mean field game approach modeling congestion and aversion in pedestrian crowds. Transp. Res. B Methodol. **45**, 1572–1589 (2011)
23. Lasry, J.-M., Lions, P.-L.: Mean field games. Jpn. J. Math. **2**(1), 229–260 (2007)
24. Leal-Taixé, L., Pons-Moll, G., Rosenhahn, B.: Everybody needs somebody: modeling social and grouping behavior on a linear programming multiple people tracker. In: IEEE International Conference on Computer Vision Workshops (ICCVW). 1st Workshop on Modeling, Simulation and Visual Analysis of Large Crowds (2011)
25. Matsumoto, M., Nishimura, T.: Mersenne twister: a 623-dimensionally equidistributed uniform pseudo-random number generator. ACM Trans. Model. Comput. Simul. **8**(1), 3–30 (1998)
26. Maury, B., Roudneff-Chupin, A., Santambrogio, F.: A macroscopic crowd motion model of the gradient-flow type. M3AS **20**(10), 1787–1821 (2010)
27. Mehran, R., Oyama, A., Shah, M.: Abnormal crowd behavior detection using social force model. In: CVPR, pp. 935–942 (2009)
28. Muramatsu, M., Nagatani, T.: Jamming transition in two-dimensional pedestrian traffic. Physica A **275**, 281–291 (2000)
29. Painter, K.: Continuous models for cell migration in tissues andï£¡applications to cell sorting via differential chemotaxis. Bull. Math. Biol. **71**, 1117–1147 (2009)
30. Pellegrini, S., Ess, A., Schindler, K., van Gool, L.: You'll never walk alone: modeling social behavior for multi-target tracking. In: International Conference on Computer Vision (2009)
31. Piccoli, B., Tosin, A.: Pedestrian flows in bounded domains with obstacles. Contin. Mech. Thermodyn. **21**(2), 85–107 (2009)
32. Schadschneider, A.: Simulation of evacuation processes using a bionics-inspired cellular automaton model for pedestrian dynamics. In: Fukui, M., Sugiyama, Y., Schreckenberg, M., Wolf, D. (eds.) Traffic and Granular Flow '01, pp. 1160–1168. Springer, Berlin/Heidelberg/Nagoya (2002)
33. Schadschneider, A., Klingsch, W., Kluepfel, H., Kretz, T., Rogsch, C., Seyfried, A.: Evacuation dynamics: empirical results, modeling and applications. In: Meyers, R.A. (ed.) Encyclopedia of Complexity and System Science, vol. 3, p. 3142. Springer, New York/London (2009)
34. Seyfried, A., Schadschneider, A.: Fundamental diagram and validation of crowd models. In: Umeo, H., Morishita, S., Nishinari, K., Komatsuzaki, T., Bandini, S. (eds.) Cellular Automata. Volume 5191 of Lecture Notes in Computer Science, pp. 563–566. Springer, Berlin/Heidelberg (2008)
35. Seyfried, A., Steffen, B., Klingsch, W., Lippert, T., Boltes, M.: The fundamental diagram of pedestrian movement revisited – empirical results and modelling. In: Schadschneider, A., Pöschel, T., Kühne, R., Schreckenberg, M., Wolf, D.E. (eds.) Traffic and Granular Flow'05, pp. 305–314. Springer, Berlin/Heidelberg (2007)
36. Simpson, M., Landman, K., Hughes, B.: Diffusing populations: ghosts or folks? Australas. J. Eng. Educ. **15**, 59–67 (2009)
37. Treuille, A., Cooper, S., Popovic, Z.: Continuum crowds. ACM Trans. Graph. **25**, 1160–1168 (2006). Proceedings of SCM SIGGRAPH 2006
38. Weidmann, U.: Transporttechnik der Fussgänger - Transporttechnische Eigenschaften des Fussgängerverkehrs (Literaturstudie). Literature Research 90, Institut füer Verkehrsplanung, Transporttechnik, Strassen- und Eisenbahnbau IVT an der ETH Zürich, March 1993. in German

39. Yamaguchi, K., Berg, A., Ortiz, L., Berg, T.: Who are you with and where are you going? In: IEEE Conference on Computer Vision and Pattern Recognition (CVPR), 2011, pp. 1345–1352, June 2011
40. Yuhaski, S.J., Jr., Smith, J.M.: Modeling circulation systems in buildings using state dependent queueing models. Queueing Syst. Theory Appl. **4**(4), 319–338 (1989)
41. Zhang, J., Klingsch, W., Schadschneider, A., Seyfried, A.: Ordering in bidirectional pedestrian flows and its influence on the fundamental diagram. J. Stat. Mech. Theory Exp. **2012**(02), P02002 (2012)